Enhancement of Microcalcifications in Digitized Mammograms: Multifractal and Mathematical Morphology Approach

Tomislav Stojić

Research Assitant
University of Belgrade
Faculty of Mechanical Engineering

Branimir Reljin

Full Professor
University of Belgrade
School of Electrical Engineering

Two methods for enhancing the microcalcifications in digitized mammograms are under consideration. First method is based on multifractal approach, and second on modern mathematical morphology. In multifractal approach, from initial mammogram image, a corresponding multifractal "images" are created, from which a radiologist has a freedom to change the level of segmentation in an interactive manner. The second method, using an appropriate combination of some morphological operations, enables high local contrast enhancement, followed by significant suppression of background tissue, irrespective of the radiology density of the tissue. By iterative procedure this method highly emphasizes only small bright details, possible microcalcifications. The interactive approach enables the physician to control the level of segmentation. Suggested methods were tested through referent mammograms from MiniMIAS database and from clinical praxis mammograms.

Keywords: medical image processing microcalcifications, mathematical morphology, multifractal analysis.

1. INTRODUCTION

Breast cancer is a leading cause of mortality in women population in developed countries [1,2]. One of the significant signs of possible cancerous changes are small calcium deposits in the breast tissue, usually referred to as microcalcifications [3]. Those anomalies may be viewed in radiology film as small spots brighter than surrounding [3,4]. Unfortunately, for several reasons: microcalcifications are small sized (typically from 0.1 up to a few of millimeters), they often appear in an inhomogeneous background tissue, and the local contrast is usually low, detection of microcalcifications is a difficult task, even for skilled radiologists.

By digitizing radiology films and applying digital image processing algorithms, significant improvements of image analysis are possible. Moreover, digital mammography, allows direct digitalization: the radiology image is converted directly to digital image. This technology can overcome many drawbacks recognized in classic film technology, but such devices are expensive and the detection of microcalcifications still remains a difficult task. Conventional contrast enhancement algorithms and thresholding [5] are not quite appropriate methods since they are pixel oriented – they globally change the whole image, not only particular details of interest, like microcalcifications. Several methods have been proposed for segmentation and/or detection of microcalcifications, such as classical image filtering [6,7], techniques based on mathematical

morphology [8,9], stochastic fractal models [10,11], wavelet analysis [12-15] and multiscale analysis [16].

In this paper the two methods for enhancing microcalcifications in digitized mammograms will be considered. One method is based on multifractal (MF) approach and the other on mathematical morphology (MM). In MF approach, the main premise was related to the fact that in normal state the human tissue is characterized by high degree of *self-similarity* [17-19]. The tissue anomalies are then considered as structural "defects", i.e. as deviations from global regularity of the background. Since the MF analysis is capable to describe image features both from local and global points of view, this analysis may be used for extracting anomalies from the background [20-24].

Mathematical morphology has been already used for digital image processing [3,25]. Morphological contrast enhancement methods proved its efficiency in fingerprint segmentation [26]. Moreover, the MM method may be used for emphasizing small sized bright details in the image, thus being capable to enhance microcalcifications [27].

In Section 2 the modified MF approach adapted to extraction of isolated bright objects in digital mammograms is described. In Section 3 the MM method is presented. The comparison between two described methods, through testing on referent mammograms from MiniMIAS (*Mammographic Image Analysis Society*) database [28] and from clinical praxis [29], is presented in Section 4. Section 5 consists of concluding remarks.

2. MODIFIED MULTIFRACTAL SEGMENTATION

2.1 Multifractal analysis basics

Many natural objects and phenomena exhibit self-similar or fractal property: a structure is assumed to be

made of parts similar to the whole, exactly or statistically. Artificially generated fractal structures are commonly known as *deterministic* (or, *mathematical*) *fractals* [17,18]. These structures are generated by using exact rules and they are characterized by the same fractal dimension in whole scales, thus they are referred to as *monofractals*. Instead, a variety of natural objects may also exhibit self-similarity but only in a statistical way. These structures are known as *random fractals*. The fractal dimension of such structures varies with the observed scale, thus they are referred to as *multifractals* [18-20].

The quantitative description of multifractal property can be derived in several ways. Very often a box-counting method is used, due to its simplicity. Let the structure S be divided into non-overlapping boxes S_i of size ε such that $S = \cup_i S_i$. Each box S_i is characterized by some amount of measure, $\mu(S_i)$, and boxes may be assumed to be measure domains. An equivalent parameter suggested to the MF analysis is defined by a quantity

$$\alpha_i = \frac{\ln(\mu(S_i))}{\ln(\varepsilon)}, \qquad (1)$$

which is known as the *coarse Hölder exponent* of the subset S_i. If ε tends to zero the coarse Hölder exponent approaches the limiting value α at observed point

$$\alpha = \lim_{\varepsilon \to 0} (\alpha_i). \qquad (2)$$

Parameter α depends on the actual position on the fractal and describes *local regularity* of the structure. In the whole structure there are usually many boxes (or points) with the same parameter α. Consequently, the next step is to find the distribution of this quantity, i.e. to find the function $f(\alpha)$, known as the MF spectrum, over subsets characterized by α. The function $f(\alpha)$ describes the *global regularity* of observed structure [18-21]. The MF spectrum can be assumed to be the *fractal dimension* over the subsets characterized by α

$$f_\varepsilon(\alpha_i) = -\frac{\ln(N_\varepsilon(\alpha_i))}{\ln(\varepsilon)}, \qquad (3)$$

where $N_\varepsilon(\alpha_i)$ is the number of boxes S_i containing a particular value of α_i. From (3) one can obtain the limiting value

$$f(\alpha) = \lim_{\varepsilon \to 0} (f_\varepsilon(\alpha)). \qquad (4)$$

The MF spectrum $f(\alpha)$ calculated as above is also known as the *Hausdorff dimension* of the distribution of α. Note again that the box-counting is only one of the several possible methods for estimation of the MF spectrum, but due to its simplicity and fast computing procedure this method is the most frequently used [20,21]. But, irrespective of particular technique for deriving MF quantities α and $f(\alpha)$, they describe both local and global regularities of the process under investigation. Consequently, MF analysis may be used in a broad class of signal processing problems, as a robust method for describing and/or extracting some features probably hidden in a large amount of data [20-24].

2.2 Multifractal analysis basics in digital image processing

Discrete space introduces several limitations in determining multifractal parameters α and $f(\alpha)$. The basic limitation is a discrete nature of box sizes covering the image space – possible size is an integer multiple of the pixel size. Instead of (1), which holds in a continuous space, in a discrete space each pixel may be characterized by a discrete set of coarse Hölder exponents as

$$\alpha_i(m,n) = \frac{\ln(\mu_i(m,n))}{\ln(i)}, \, i = 1, 2, 3, ..., \qquad (5)$$

where $\mu_i(m,n)$ is the amount of a measure within observed box size $\varepsilon = i$, and (m,n) are discrete spatial coordinates. The limiting procedure given by (2) and (4), meaning $\varepsilon \to 0$, is not possible in discrete space since the minimal size is $\varepsilon_{min} = 1$. Moreover, quantities α and $f(\alpha)$ are even undefined if $\varepsilon = \varepsilon_{min} = 1$. Instead, we may estimate these quantities indirectically, from bi-logarithmic diagrams. For estimating Hölder exponents we can calculate natural logarithms of measure value, $\ln(\mu_i(m,n))$, and of the box size, $\ln(i)$, and plot corresponding points in bi-logarithmic diagram $\ln(\mu_i(m,n))$ vs. $\ln(i)$. Then, the limiting value of $\alpha(m,n)$ is estimated as a slope of linear regression line in the log-log space [30].

After finding the values of α we may create an "α-image" – a matrix of the same dimension as initial image but filled by the values of $\alpha(m,n)$ with one-by-one correspondence to image pixels. From this matrix, the MF spectrum $f(\alpha)$, also in a matrix form, $f(m,n) = f(\alpha(m,n))$, is estimated as follows. First, continuous Hölder exponents are discretized into R values of α_r:

$$\alpha_r = \alpha_{min} + (r-1)\Delta\alpha_r, r = 1, 2, ..., R. \qquad (6a)$$

We used the uniform division with

$$\Delta\alpha_r = \Delta\alpha = (\alpha_{max} - \alpha_{min})/R. \qquad (6b)$$

If the actual value of α is within the subrange r, i.e., if $\alpha_r \le \alpha < (\alpha_r + \Delta\alpha)$, it is replaced by α_r. Such α-image is covered by a regular grid of boxes with integer box sizes $j = 1,2,...$ The boxes containing at least one value of α_r are counted, giving the number $N_j(\alpha_r)$. Boxes of different sizes are recursively taken into account and corresponding Hausdorff measures are calculated for each image pixel according to (3) as

$$f_j(\alpha_r) = -\frac{\ln N_j(\alpha_r)}{\ln(j)}, \, j = 1, 2, ... \qquad (7)$$

The dimension of boxes in (7) is denoted as j, instead of i used in (5), indicating to different domains: i relates to pixel neighborhood in image domain, while j relates to size of regular grid into α-matrix domain.

Finally, from a set of discrete points in bi-logarithmic diagram of $\ln N_j(\alpha_r)$ vs. $-\ln(j)$, the MF spectrum $f(\alpha)$ is estimated from linear regression, in similar manner as in case of estimation of α. The procedure is repeated for whole the α-matrix thus obtaining "$f(\alpha)$-image" – a matrix filled by pixel-wise values of $f(\alpha)$ with one-by-

one correspondence with pixel positions in initial image. This procedure is described in details in [30].

Different measures $\mu_i(m,n)$, may be used for estimating α. Some of the most frequently used measures are [20]:

$$\text{Maximum: } \mu_i(m,n) = \max_{(k,l) \in \Omega} g(k,l), \qquad (8a)$$

$$\text{Minimum: } \mu_i(m,n) = \min_{(k,l) \in \Omega^*} g(k,l), \qquad (8b)$$

$$\text{Sum: } \mu_i(m,n) = \sum_{(k,l) \in \Omega} g(k,l), \qquad (8c)$$

where: i is a size of a measure domain around observed pixel (m,n), Ω is a set of all pixels (k,l) within a measure domain, and $g(k,l)$ is a grayscale intensity at point (k,l). Certainly, different measures lead to different Hölder exponents and may be used to produce different effects on the processed image.

2.3 Adaptation of multifractal analysis to segmentation of microcalcifications

By appropriate choice of a pair α and $f(\alpha)$, different image features may be extracted and/or enhanced [20-24]. In radiology image, the microcalcifications are seen as small bright and relative smooth surfaces not belonging to surrounding, with a small gray-level variation. Sharp change in gray-level arises just around the edge of microcalcification [31,32]. But, if microcalcifications are located in radiology "dense" tissue, which strongly reflects X-rays, the contrast between them and surrounding tissue is very low, making their detection difficult even for skilled radiologists.

Having in mind the main features of microcalcifications: (*i*) they are small parts brighter then surrounding tissue, (*ii*) not belonging to background tissue (rare events), with (*iii*) a relatively high local contrast, having (*iv*) different size and shape, and (*v*) usually clustered, we can infer the guidelines for adaptation of multifractal analysis targeted to segmentation of microcalcifications. From an MF image with one-by-one pixel-wise correspondence with an original image, we should be able to select possible microcalcifications as image pixels having high α (high local contrast) and low $f(\alpha)$ (rare events). In [30] it was shown that the capacity measure "Minimum", given by (8b), applied to an inverted (negative) image, is well suited to emphasizes local image regularity. Namely, for negative image bright anomalies (possible microcalcifications) migrate to dark region, and in this region the local contrast, described by the ratio $\Delta \ln(\mu)/\Delta\mu$ is very high. In this way, we obtain the effect of "logarithmic amplifier", which strongly enhances just small gray level variations in the dark zone of inverted image (bright zone of an original image). This procedure does not reduce the sensitivity within regions in the middle gray, while in the bright zone of inverted image (dark zone in an original image) a contrast between microcalcifications and surrounding tissue is naturally high, as approved in [30].

Considering the feature (*iv*), we found that disk-shaped domains are well suited to most of microcalcifications. The multifractal spectrum is determined by box-counting method according to (7). The box sizes may vary from $j = 1$ (one α pixel) to $j = \max(M,N)$ (a whole α-image of size $M \times N$). Since our goal is to favor small singularities, i.e., high frequency components in α distribution, we used small boxes sized $j = 1$ to $j = 16$ α-pixels. Namely, by the increasing of the box size, the number of the nonempty boxes decreases. However, if the box size is large enough the number of nonempty boxes tends to saturation: it may remain unchanged through the box size increases. Then, points on bi-logarithmic plot $\ln N_j(\alpha_r)$ vs. $-\ln(j)$ stay on horizontal line, significantly reducing the resolution of calculated $f(\alpha)$ values. On the contrary, by using smaller boxes, the number of nonempty boxes significantly varies with the box dimension change, preventing saturation and enabling high resolution of estimated $f(\alpha)$ values [30].

The number of α subranges, denoted as R in (6), also influences the accuracy of multifractal spectrum. A small number of subranges has an effect of low-frequency filtering, yielding to smooth spectrum but with small resolution and small "sharpness". Conversely, too much subranges produce saw-toothed ("erratic") spectrum, with more details. In our research, as a compromise solution, the value of $R = 100$ is adopted.

3. MORPHOLOGY SEGMENTATION

3.1 Basics of mathematical morphology

The morphological image processing techniques are based on modern mathematical set theory [25]. The morphological operations have been originally developed for the analysis of binary (black and white) images, and later extended to monochrome (gray-scale) and multicomponent (color) images [5]. Morphological operations are based on the relationships between the two sets: an input image matrix, I, and a processing operator, so-called the structuring element, S, which is usually much smaller than the input image. Although the pixels of structuring element may have arbitrary values, the most commonly used is the *flat* structuring element, having the same values of all nonzero pixels. By selecting the shape and size of structuring element, different results may be obtained in output image.

Two morphological operations: *dilation* and *erosion* are fundamental to morphological processing. The dilation of a two-dimensional gray-scale digital image, $I(m,n)$, by a two-dimensional flat structuring element, $S(i,j)$, is defined as [5]:

$$(I \oplus S)(m,n) = \max\{I(m-i,n-j)\}, \qquad (9)$$

with $[(m-i),(n-j)] \in D_I$ and $(i,j) \in D_S$, where D_I and D_S are the domains of I and S, respectively. The origin of S is assumed to coincide with the actual current position (m,n) of the input image. This way the pixel element at point (m,n) is simply replaced by the maximum value of image pixels covered by the nonzero members of the structuring element. The output image tends to be brighter than the input, and dark details are reduced or completely removed, depending on how their values and shapes relate to the structuring element used.

Gray-scale erosion is defined as:

$$(I \ominus S)(m,n) = \min\{I(m+i, n+j)\}, \qquad (10)$$

assuming $[(m+i),(n+j)] \in D_I$ and $(i,j) \in D_S$, where D_I and D_S are the domains of I and S, respectively. The condition that $(m+i)$ and $(n+j)$ have to be in the domain of I, and i and j have to be in the domain of S, denotes that the structuring element is covered by I. The erosion results in replacing pixel values with the minimum value of image pixels within the domain defined by the size and shape of the structuring element. The output image tends to be darker than the input and the bright details in the input image are reduced or removed, depending on how their values and shapes relate to the structuring element.

The next two, very important morphological operations, are *opening* and *closing*. The opening of image I by a structuring element S is defined as erosion followed by dilation, while closing has the opposite order of these operations:

$$I \circ S = (I \ominus S) \oplus S, \text{ opening} \qquad (11)$$

$$I \bullet S = (I \oplus S) \ominus S, \text{ closing.} \qquad (12)$$

As a consequence, with gray-scale opening one can remove bright details smaller than the structuring element used. Large details, both bright and dark, which are larger than the structuring element, remain nearly unchanged. Conversely, closing operation removes dark details smaller than the structuring element.

By combining morphological opening and closing, various image processing tasks can be performed. Enhancing (or suppressing) details smaller than structuring element may be obtained by morphological operations known as *top-hat* (TH) and *bottom-hat* (BH) transformation. The *top-hat* transformation is obtained by subtracting a morphologically opened image from the original one:

$$TH = I - (I \circ S). \qquad (13)$$

As already mentioned, by gray-scale opening one can remove the bright details from an input image, smaller than used structuring element. Subtracting an opened image from the original one yields an image, which emphasizes the features removed by opening. Thus, *TH* transformation is an excellent tool for enhancing small bright details from a nonuniform background, and it has proved its efficiency in fingerprint segmentation applications [26].

The morphological *bottom-hat* transformation is defined as a difference between a morphologically closed image and an original image:

$$BH = (I \bullet S) - I. \qquad (14)$$

Consequently, this transformation produces an effect opposite to the *top-hat* transformation. That means, by using closing instead of opening, and subtracting the original image from the closed one, one can extract dark features from a brighter background. Note that both transformations equalize a nonuniform background illumination.

3.2 Local contrast enhancement using morphological operations

Local contrast enhancement can be achieved by adding an original image to the difference between top-hat and bottom-hat transformed image. The output image called the *contrast image*, C, is given by:

$$C = I + (TH - BH). \qquad (15)$$

By the difference $(TH - BH)$, bright details, smaller than the structuring element, are strongly emphasized, while dark details are suppressed. Furthermore, if we add an original image to this difference a high-frequency filtering is achieved. Consequently, the enhancement of bright details smaller than the structuring element S is reinforced, and uneven background (surrounding tissue texture) is highly equalized. This procedure can be iteratively repeated, by using the output image from the k-th iteration as the input image for the next, $(k+1)$-th, iteration, i.e., by

$$I^{(k+1)} = C^{(k)}, k = 1, 2, 3, ..., \qquad (16)$$

and repeating the procedure described by (13) to (15). The proposed method converges very rapidly. Our intensive simulations showed that not more than three iterations are sufficient. The transformed image, obtained after convergence, contains only small bright details, while uneven background tissue is equalized.

By an appropriate selection of shape and size of the structuring element, as well as the number of necessary iterations, the proposed algorithm may be customized to particular processing tasks.

3.3 Visualization of microcalcifications in mammograms

The iterative procedure for local contrast enhancement, described by (15) and (16), started with the structuring element whose size is close to expected upper limit of microcalcifications dimension (about 2.5 mm) [3]. The size of structuring element appropriately decreases with subsequent iterations, since once finding the possible microcalcification we tried to detect its peak, according to typical feature of microcalcifications, described in [32].

The final segmentation of microcalcifications is obtained by thresholding applied to the output image after k-th iteration, $C^{(k)}$. First, the magnitudes of all pixel values in output image are normalized to the range [0-1]. After that, by choosing the proper threshold value, T, one can extract bright details (microcalcifications candidates) from the background. Any pixel with a gray level L, larger than T is labeled white (corresponding to the normalized value 1), while other pixels are labeled black (the value of 0). In this way, the extracted details are presented as white islands in the black surrounding. The contour lines of the segmented bright objects may be extracted and superimposed onto the original, indicating to (possible) microcalcifications. This thresholding procedure may be performed in an interactive manner allowing adjustment of the threshold level T for finding the best result.

4. COMPARISON OF TWO METHODS

The efficiency of suggested methods is verified through referent mammograms from public domain MiniMIAS database [28]. MiniMIAS database has been derived from MIAS (*Mammographic Image Analysis Society*) database [33]. Films are taken from the UK National Breast Screening Programme. All mammograms are in medio-lateral (ML) oblique view and were digitized to 50×50 micron resolution. The images have been reviewed by the consultant radiologists and anomalies have been identified and marked: the location of the anomaly and the radius of a circle which encloses it. Images from MIAS database were rescaled from 50 to 200 microns per pixel forming publicly available MiniMIAS database. All mammograms in the MiniMIAS database have the same size of 1 MB, same dimension (1024×1024 pixels) and same gray-level range (from 0 – black to 255 – white).

4.1 Radiology easy case

Figure 1a represents full-sized mammogram (1024×1024 pixels) mdb219.pgm from MiniMIAS database and its part (128×128 pixels), Figure 1b, around clinically approved microcalcifications (under the white circle in Figure 1a). This case belongs to an "easy" one, since the tissue is radiology sparse and microcalcifications are visible even for not so skilled radiologist. Figures 1a and 1b clearly confirm basic features of microcalcifications: they are small bright anomalies – parts in a mammogram not belonging to background tissue. In geometrical interpretation, they are seen as singular sets of points. From the multifractal standpoint they are characterized by both high α and low $f(\alpha)$ values, because, they represent sharp local changes and globally rare events [20-22]. The MF spectrum $f(\alpha)$ is depicted in Figure 1c, while α and $f(\alpha)$ images are presented in Figures 1d and 1e, respectively.

In Figure 1d the edges of microcalcifications are represented as white pixels (high α values) while in Figure 1e the edges are black (low $f(\alpha)$ values). Note that in α-image the background is characterized by low α-values (dark regions, although the background is not pure black).

In order to extract microcalcifications we have to choose image pixels characterized by high values of α and low values of $f(\alpha)$. Referring to multifractal spectrum in Figure 1c, if we select image pixels from desired range of $f(\alpha)$ values: $f_1 \leq f(\alpha) < f_2$, and refine the segmentation by using successive morphological closing and opening procedures, we can obtain contour lines around segmented details. These contour lines have been superimposed to the original image and displayed as in Figure 1f, for $0 \leq f(\alpha) < 0.4$, strongly indicating to a cluster of microcalcifications. By changing $f(\alpha)$ range, we can interactively choose the appropriate segmentation level for each particular case, as depicted in Figure 1g.

Figure 2a shows the output image $C^{(3)}$, obtained by applying the morphology segmentation after $k = 3$ iterations. The iterative image processing is performed following (15) and (16) using only the pixels within the segmented breast tissue region. Disk shaped structuring element of 5 pixels radius was used in the first iteration (corresponding to the microcalification diameter of about 2.25 mm). Microcalcifications are highly enhanced, while background tissue is equalized and homogenized. Figure 2b shows the original image with superimposed microcalcifications contour lines. Contour lines are extracted from the normalized image $C^{(3)}$ by applying the threshold of $T = 0.4$. For better visualization, a zoomed detail of the size 256×256 pixels is presented in Figure 2c.
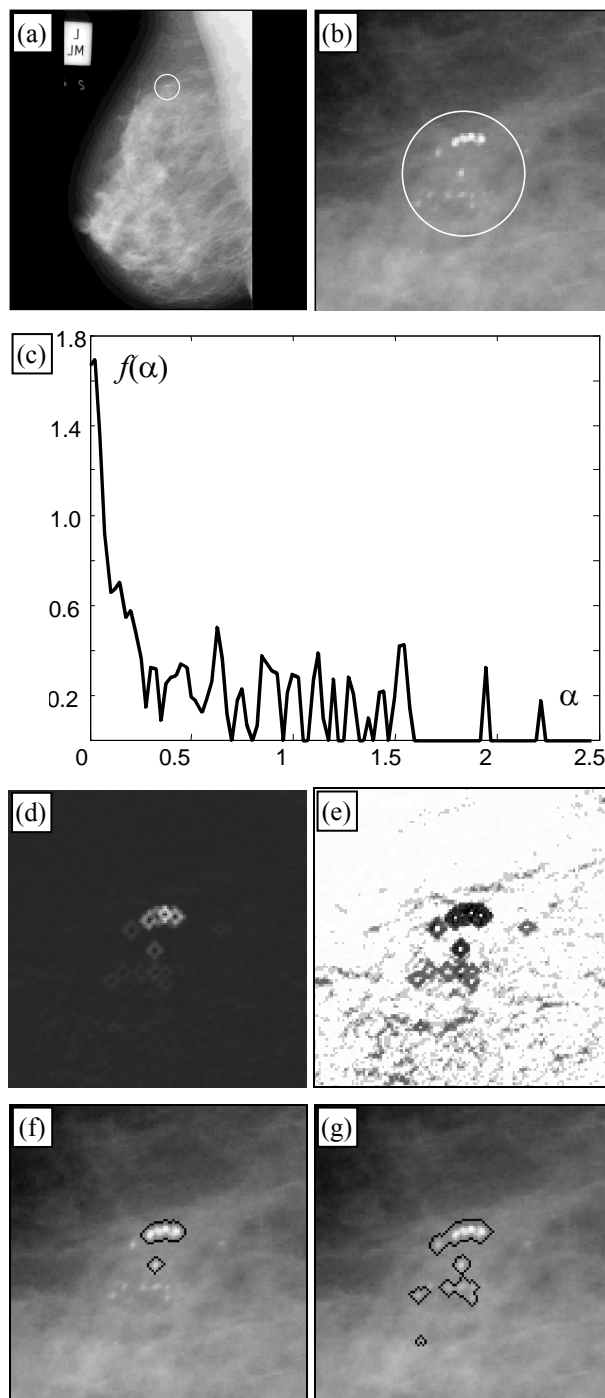

Figure 1. Multifractal segmentation: (a) mammogram mdb219.pgm from MiniMIAS database and (b) its selected part around clinically approved microcalcifications, (c) an MF spectrum of an image from Figure 1b, (d) α image, (e) corresponding *f(α)* image of image from Figure 1b and (f) and (g) superimposed contour lines around segmented details for 0 ≤ *f(α)* < 0.4 and 0 ≤ *f(α)* < 0.6, respectively
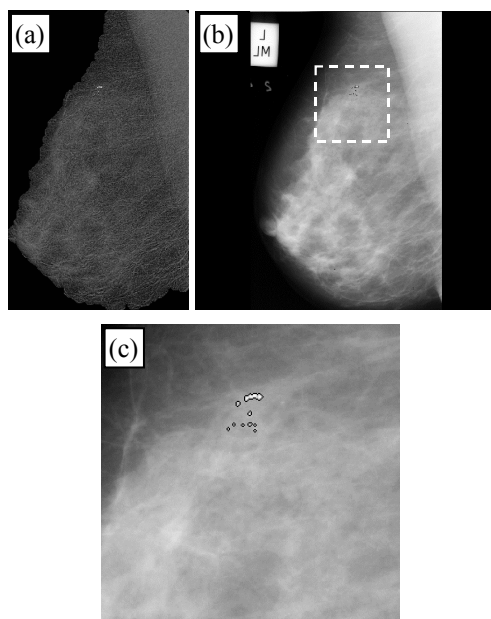
Figure 2. Morphology segmentation: (a) transformed image $C^{(3)}$ after three iterations, (b) mammogram mdb219 with superimposed microcalcifications contour lines (threshold $T = 0.4$) and (c) zoomed detail of size 256 × 256 pixels corresponding to the white rectangle from Figure 2b

4.2 Radiology hard case

A mammogram mdb253.pgm from MiniMIAS database is shown in Figure 3a. Clinically approved microcalcifications are located within a small black circle. A part of this mammogram (256 × 256 pixels) around approved microcalcifications is presented in Figure 3b. The breast tissue is very dense causing very poor contrast between anomalies and surrounding tissue. Thus, the visual detection of microcalcifications is extremely difficult even for skilled radiologists. The corresponding $f(\alpha)$ image obtained from the image in Figure 3b is shown in Figure 3c. Superimposed contour lines around pixels from Figure 3b characterized by $0 \leq f(\alpha) < 0.3$ are plotted in Figure 3d. As we can conclude, clinically approved microcalcifications are highly visible.

Morphology transformed image $C^{(3)}$ of the breast region from Figure 3a, after three iterations described by (15) and (16), is shown in Figure 4a. Due to extremely low contrast, visual detection of the enhanced microcalcifications is still difficult. But, after applying the thresholding on the $C^{(3)}$ image, microcalcifications may be extracted as shown in Figure 4b. The contour lines are obtained from $C^{(3)}$ after applying the threshold of $T = 0.65$. Besides verified microcalifications, we segmented other anomalies, possible microcalcifications, outside from declared region – signed by black arrows in Figure 4b.

4.3 Mammogram with high masking effect caused by background tissue

As a third example, we will observe a mammogram mdb223.pgm from MiniMIAS database as shown in Figure 5a. Clinically approved microcalcifications are located somewhere within small black circles. A part of this mammogram (256 × 256 pixels) around approved

microcalcifications is presented in Figure 5b. Microcalcifications are visible for radiologists, but automated selection is not so simple since background tissue has similar local contrast producing masking effect. However, both of our algorithm may extract very efficiently regions containing microcalcifications without affecting background tissue, as shown in Figures 5c and 5d. In Figure 5c the segmentation results of MF method by making contour lines around extracted details for $0 \leq f(\alpha) < 0.4$, is depicted. The same part of mammogram, shown in Figure 5b, is morphology segmented and obtained results are shown in Figure 5d. Black arrow indicates to possible macrocalcification.
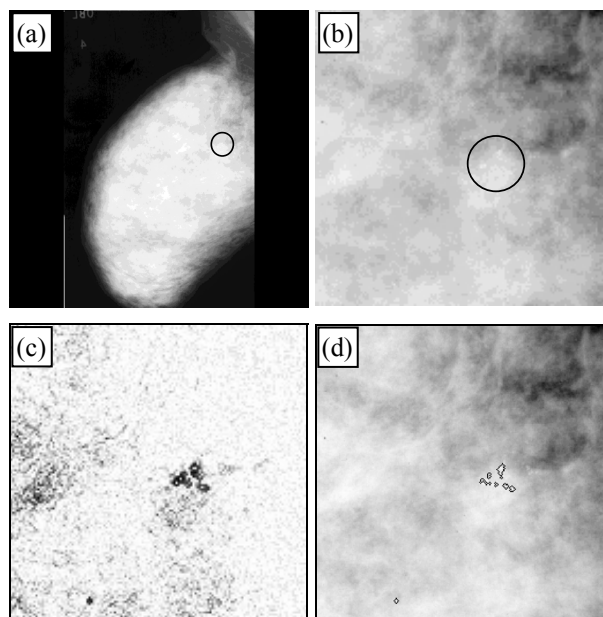

Figure 3. (a) original mammogram mdb253.pgm from MiniMIAS database and (b) its selected part (256 × 256 pixels) around clinically approved microcalcifications, (c) multifractal segmentation – $f(\alpha)$ image of image in Figure 3b and (d) multifractal segmentation – superimposed contour lines around pixels from Figure 3c having $0 \leq f(\alpha) < 0.3$
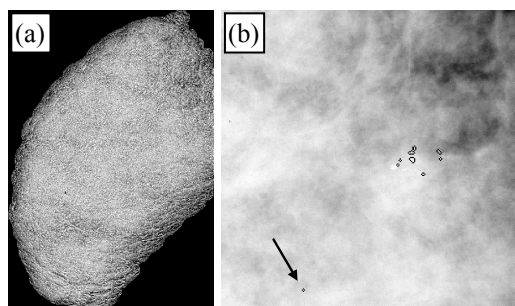

Figure 4. Morphology segmentation: (a) morphology transformed image $C^{(3)}$ after three iterations and (b) superimposed contour lines around segmented details for threshold of $T = 0.65$

4.4 Mammogram from clinical praxis

The last example, mammogram r21.tif, depicted in Figure 6a, is from clinical praxis from Clinical Center "Bezanijska kosa" in Belgrade, Serbia. The film digitalization was adjusted to 600 dpi (43 micrometers per pixel). Notice that mammogram is cranio-caudal (CC) oblique view. We analyzed only a part of mammogram within superimposed white dashed square.

Results after MF and MM segmentation are shown in Figures 6b and 6c, respectively. According to increased mammogram resolution compared to MiniMIAS database (43 micrometers vs. 200 micrometers), disk shaped structuring element of 25 pixels radius was used (corresponding to the microcalification diameter of about 2.2 mm).
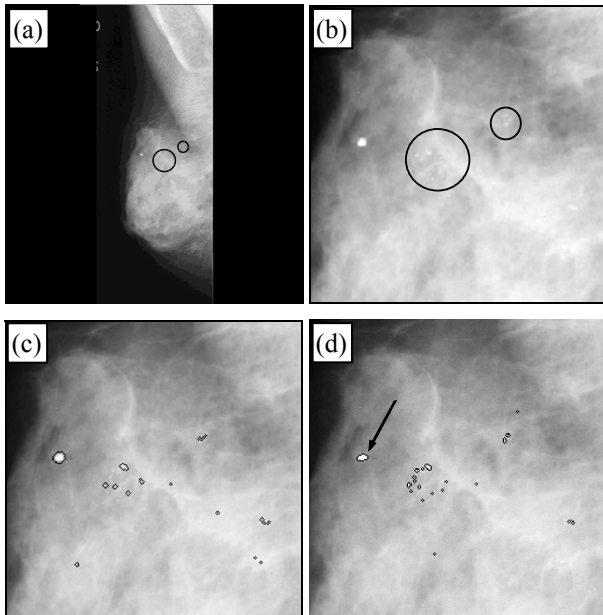

Figure 5. (a) original mammogram mdb223.pgm from MiniMIAS database and (b) its selected part (256 × 256 pixels) around clinically approved microcalcifications, (c) multifractal segmentation – superimposed contour lines around segmented details from image in Figure 5b having 0 ≤ $f(\alpha)$ < 0.4 and (d) morphology segmentation – superimposed contour lines for threshold of T = 0.65
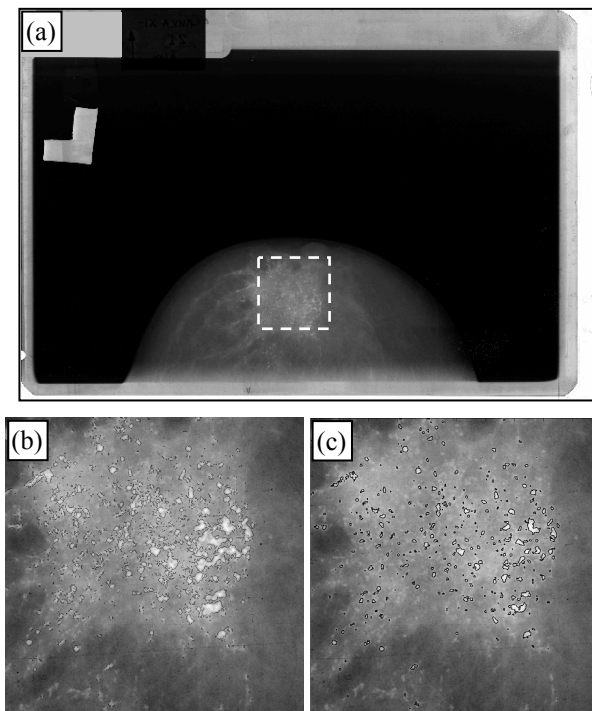

Figure 6. (a) mammogram r21.tif from clinical praxis, (b) superimposed contour lines after segmentation of mammogram part within white dashed square by multifractal method for 0 ≤ $f(\alpha)$ < 0.4 and (c) superimposed contour lines after segmentation of mammogram part within white dashed square by morphology method for threshold T = 0.65

4.5 Comparison between multifractal and morphological method

Both described methods emphasize anomalies in mammograms brighter than the surrounding tissue. The multifractal approach recognizes microcalcifications as "defects" in the surrounding tissue structure. Morphology based method uses appropriate combination of morphology transformations to enhance local contrast and reduce background tissue texture. Different basic principles of these methods cause different way of anomaly segmentation.

Multifractal method extracts details have significantly lower multifractal dimension than their surrounding. Microcalcification, by itself, is a relatively homogenous small bright surface in a mammogram. As we already mentioned, a sharp change in gray-level arises just around the edge of microcalcification. First, we invert mammogram, moving bright anomalies to the dark region and putting them under strong influence of the "logarithmic amplifier". This amplified local contrast causes suddenly changes in measure values by increasing measure domain, producing relatively high values of α coefficients just around the microcalcification. However, the pixels within strong textured tissue often have high α coefficients, too. To distinguish anomalies from highly textured tissue, we determine fractal dimension of α image. The pixels within textured tissue are frequent events in a mammogram, causing their fractal dimension be greater than 1, $f(\alpha) > 1$, because by the decreasing of the covering box size overall number of the nonempty boxes proportionally increases [30]. On the other hand, the tissue anomalies are rare events, having small fractal values, $f(\alpha) \leq 0.5$, since by decreasing of the covering box size overall number of the nonempty boxes remains practically unchanged [30]. Microcalcification, by itself, occupies small area in a mammogram, and by splitting larger covering boxes into smaller ones, the overall number of nonempty boxes (e.g. boxes overlapping with microcalification area) increases very slowly. This causes small slope of fitting line in bi-logarithmic plot used for $f(\alpha)$ estimation.

Mutifractal segmentation emphasizes the contour around microcalcification, because the points lying on this boundary have at the same time very high α and very low $f(\alpha)$ values. Therefore, microcalcifications are segmented from multifractal images as those area of pixels, which have both high α and low $f(\alpha)$ values.

Morphology based method emphasizes microcalcifications by direct increasing of local contrast using appropriate combination of top-hat and bottom-hat transformation. This method enhances the brightest area within the microcalcification surface in a mammogram. Although microcalcification represents small relatively homogenous surface, there is small brightness (gray-level) decreasing by moving from center of microcalcification toward its periphery. The presence of this brightness gradient has been exploited in [32] for successful simulation of microcalcifications. Morphological method enhances this brightness gradient, remaining its central (the brightest) part unchanged, while eroding its peripheral area. Due to this, morphology segmented details looks "eroded" and area under contour lines around them is smaller than in

multifractal segmentation. This was expected, because multifractal method segments boundary line around microcalcification, while morphology method segments its brightest, central area.

It should be noticed that, due to its simplicity, the morphological method is much faster than the multifractal one. Morphology method is suitable for real time mammogram processing. On the other hand, when once creating multifractal images, one can extract not only singular details (in this case microcalifications) from a mammogram, but also the other image features, like edges, texture areas, flat areas, etc., by appropriate selection of desired range of α and/or $f(\alpha)$.

5. CONCLUSION

Our research was addressed to the extraction of microcalcifications in digital mammograms. In original image domain, microcalcifications are represented by small bright spots not belonging to background tissue, usually in the form of clusters, and characterized by sharp change of local contrast just at their edges.

In multifractal terminology these features are described both by high values of Hölder exponent α (high local changes) and low values of its distribution $f(\alpha)$ (rare events in global sense). Multifractal analysis is adapted to enhance small contrast changes permitting very good detection of calcifications even in radiology dense tissue when classical visual detection and/or image processing algorithms fall down. After obtaining multifractal image a radiologist has the freedom to change the level of segmentation in interactive way, by setting the range of $f(\alpha)$ values, and to find regions which may contain microcalcifications.

It is also shown that the local contrast enhancement followed by high suppression of surrounding tissue can be achieved using an appropriate combination of morphological top-hat and bottom-hat transformations. By a proper choice of shape and size of structuring element, the proposed algorithm may be customized to the particular processing task. Iterative application of the proposed method highly enhances small, bright details and suppresses the background tissue. This is suitable for mammogram analysis, since tissue microcalcifications, which are often an early breast cancer sign, are usually displayed as bright areas in a mammogram due to their high attenuation of X-rays. The simulation of the proposed method suggested that three iterations are quite sufficient for extracting desired details. The final segmentation is obtained by thresholding the processed output image. By an appropriate choice of the threshold, one can extract desired bright details from the background and then segment their contour lines.

By superimposing contour lines onto the original mammogram in both methods, visualization of the segmented bright details is highly improved. This procedure may be performed in an interactive manner to allow adjustment of threshold level for the best results.

The efficiency of both proposed method was tested through public domain mammograms from MiniMIAS database and from clinical praxis. In all tested cases the proposed methods successfully detected microcalcifications, previously confirmed by a radiologist.

REFERENCES

[1] Boring, C.C., Squires, T.S. and Tong, T.: Cancer statistics, 1992, CA: A Cancer Journal for Clinicians, Vol. 42, No. 1, pp. 19-38, 1992.

[2] Tabar, L., Duffy, S.W. and Burhenne, L.W.: New Swedish breast cancer detection results for women aged 40-49, Cancer, Vol. 72, No. S4, pp. 1437-1448, 1993.

[3] Suri, J.S., Kamaledin Setarehdan, S. and Singh, S. (Eds.): *Advanced Algorithmic Approaches to Medical Image Segmentation*, Springer, London, 2002.

[4] Bronzino, J.D.: *The Biomedical Engineering Handbook*, CRC Press, Boca Raton, 1995.

[5] Gonzalez, R.C. and Woods, R.E.: *Digital Image Processing (Third Edition)*, Prentice Hall, Upper Saddle River, 2008.

[6] Davies, D.H. and Dance, D.R.: Automatic computer detection of clustered calcifications in digital mammograms, Physics in Medicine and Biology, Vol. 35, No. 8, pp. 1111-1118, 1990.

[7] Soni, T., Zeidler, J.R. and Ku, W.H.: Performance evaluation of 2-D adaptive prediction filters fordetection of small objects in image data, diction filters for detection of small objects in image data, IEEE Transactions on Image Processing, Vol. 2, No. 3, pp. 327-340, 1993.

[8] Dengler, J., Behrens, S. and Desaga, J.F.: Segmentation of microcalcifications in mammograms, IEEE Transactions on Medical Imaging, Vol. 12, No. 4, pp. 634-642, 1993.

[9] Zhao, D.: Rule-based morphological feature extraction of microcalcifications in mammograms, in: Acharya, R.S. and Goldgof, D.B. (Eds.): *Biomedical Image Processing and Biomedical Visualization*, SPIE, Bellingham, pp. 702-715, 1993.

[10] Lefebvre, F., Benali, H., Gilles, R., Kahn, E. and di Paola, R.: A fractal approach to the segmentation of microcalcifications in digital mammograms, Medical Physics, Vol. 22, No. 4, pp. 381-390, 1995.

[11] Li, H., Liu, K.J.R. and Lo, S.-C.B.: Fractal modeling and segmentation for the enhancement of microcalcifications in digital mammograms, IEEE Transactions on Medical Imaging, Vol. 16, No. 6, pp. 785-798, 1997.

[12] Brzakovic, D.P., Brzakovic, P. and Neskovic, M.: Approach to automated screening of mammograms, in: Acharya, R.S. and Goldgof, D.B. (Eds.): *Biomedical Image Processing and Biomedical Visualization*, SPIE, Bellingham, pp. 690-701, 1993.

[13] Wang, T.C. and Karayiannis, N.B.: Detection of microcalcifications in digital mammograms using wavelets, IEEE Transactions on Medical Imaging, Vol. 17, No. 4, pp. 498-509, 1998.

[14] Lado, M.J., Tahoces, P.G., Méndez, A.J., Souto, M. and Vidal, J.J.: A wavelet-based algorithm for detecting clustered microcalcifications in digital mammograms, Medical Physics, Vol. 26, No. 7, pp. 1294-1305, 1999.

[15] Bazzani, A., Bevilacqua, A., Bollini, D., Brancaccio, R., Campanini, R., Lanconelli, N., Riccardi, A., Romani, D. and Zamboni, G.: Automatic detection of clustered microcalcifications in digital mammograms using an SVM classifier, in: *Proceedings of the European Symposium on Artificial Neural Networks – ESANN 2000*, 26-28.04.2000, Bruges, Belgium, pp. 195-200.

[16] Netsch, T. and Peitgen, H.-O.: Scale-space signatures for the detection of clustered microcalcifications in digital mammograms, IEEE Transactions on Medical Imaging, Vol. 18, No. 9, pp. 774-786, 1999.

[17] Mandelbrot, B.B.: *The Fractal Geometry of Nature*, W.H. Freeman, Oxford, 1983.

[18] Evertsz, C.J.G. and Mandelbrot, B.B.: Multifractal measures, in: Peitgen, H.-O., Jürgens, H. and Saupe, D.: *Chaos and Fractals*, Springer, London, pp. 921-954, 1992.

[19] Iannaccone, P.M. and Khokha, M. (Eds), *Fractal Geometry in Biological Systems*, CRC Press, Boca Raton, 1996.

[20] Lévy Véhel, J. and Mignot, P.: Multifractal segmentation of images, Fractals, Vol. 2, No. 3, pp. 371-377, 1994.

[21] Lévy Véhel, J.: *Introduction to the Multifractal Analysis of Images*, Technical report, INRIA, Le Chesnay, 1996.

[22] Turner, M.J., Blackledge, J.M. and Andrews, P.R.: *Fractal Geometry in Digital Imaging*, Academic Press, San Diego, 1998.

[23] Reljin, I.S. and Reljin, B.D.: Fractal geometry and multifractals in analyzing and processing medical data and images, Archive of Oncology, Vol. 10, No. 4, pp. 283-293, 2002.

[24] Pesquet-Popescu, B. and Lévy Véhel, J.: Stochastic fractal models for image processing, IEEE Signal Processing Magazine, Vol. 19, No. 5, pp. 48-62, 2002.

[25] Serra, J.: *Image Analysis and Mathematical Morphology*, Academic Press, London, 1982.

[26] Mosorov, V.: Using tophat transformation for image fingerprints segmentation, in: *Proceedings of the International Conference on Signals and Electronic Systems – ICSES 2001*, 18-21.09.2001, Lodz, Poland, pp. 241-246.

[27] Stojić, T. and Reljin, B.: Enhancing of microcalcifications in mammograms by using morphological procedure, in *Proceedings of the 11. Conference TELFOR*, 25-27.11.2003, Belgrade, Serbia, Paper on CD, (in Serbian).

[28] Suckling, J.: *The mini-MIAS database of mammograms*, Mammographic Image Analysis Society – MIAS.

[29] Milosevic, Z.: Breast cancer diagnosis: Current status in Serbia, in: *European School of Oncology Advanced Course: Breast Cancer Screening – Quality Issues in Detection and Diagnosis*, 27-28.06.2005, Niš, Serbia, pp. 87-92.

[30] Stojić, T., Reljin, I. and Reljin, B.: Adaptation of multifractal analysis to segmentation of microcalcifications in digital mammograms, Physica A: Statistical Mechanics and its Applications, Vol. 367, pp. 494-508, 2006.

[31] Bakic, P.R., Albert, M., Brzakovic, D. and Maidment A.D.: Mammogram synthesis using a 3D simulation. II. Evaluation of synthetic mammogram texture, Medical Physics, Vol. 29, No. 9, pp. 2140-2151, 2002.

[32] Carton. A.-K., Bosmans, H., Van Ongeval, C., Souverijns, G., Rogge, F., Van Steen, A. and Marchal, G.: Development and validation of a simulation procedure to study the visibility of micro calcifications in digital mammograms, Medical Physics, Vol. 30, No. 8, pp. 2234-2240, 2003.

[33] Suckling, J., Parker, J., Dance, D., Astley, S., Hutt, I., Boggis, C., Ricketts, I., Stamatakis, E., Cerneaz, N., Kok, S., Taylor, P., Betal, D. and Savage, J.: *The Mammographic Images Analysis Society Digital Mammogram Database*, Excerpta Medica, Bridgewater, 1994, mias@sv1.smb.man.ac.uk

ИСТИЦАЊЕ МИКРОКАЛЦИФИКАЦИЈА У ДИГИТАЛНИМ МАМОГРАМИМА: МУЛТИФРАКТАЛНИ И МОРФОЛОШКИ ПРИСТУП

Томислав Стојић, Бранимир Рељин

Приказана су два метода истицања микрокалцификација у дигиталним мамограмима. Први метод заснован је на мултифракталној анализи дигиталне слике, а други на примени модерне математичке морфологије. У мултифракталном приступу креирају се мултифракталне „слике" изворног мамограма, на основу којих се даље интерактивно бира ниво сегментације детаља. Други метод, погодном комбинацијом морфолошких операција, повећава локални контраст уз снажно потискивање позадинске текстуре, независно од радиолошке густине ткива дојке. Итеративним поступком морфолошки метод високо истиче само мале детаље сјајније од околног ткива, потенцијалне микрокалцификације. Интерактивни приступ код оба метода омогућава радиологу да контролише ниво издвајања детаља. Предложени методи су тестирани на референтним мамограмима из миниМИАС базе и из клиничке праксе.